ISSN 1070-3284, Russian Journal of Coordination Chemistry, 2024, Vol. 50, No. 7, pp. 440–457. © Pleiades Publishing, Ltd., 2024.

Complexes $R_2Sn(IV)L$ with Tridentate O,N,O'-Donor Schiff Bases: Photophysical Properties and Biological Activity

D. A. Burmistrova[a], N. P. Pomortseva[a], K. D. Pashaeva[a], M. P. Polovinkina[a], N. R. Al'myasheva[b], F. M. Dolgushin[c], E. D. Tselukovskaya[d], I. V. Anan'ev[c], O. P. Demidov[e], A. I. Poddel'skii[f], N. T. Berberova[a], I. L. Eremenko[c], and I. V. Smolyaninov[a, *]

[a] *Astrakhan State Technical University, Astrakhan, Russia*

[b] *Gause Institute of New Antibiotics, Russian Academy of Medical Sciences, Moscow, Russia*

[c] *Kurnakov Institute of General and Inorganic Chemistry, Russian Academy of Sciences, Moscow, Russia*

[d] *National Research University Higher School of Economics, Moscow, Russia*

[e] *North Caucasian Federal University, Stavropol, Russia*

[f] *Institute of Inorganic Chemistry, University of Tübingen, Tübingen, Germany*

**e-mail: ivsmolyaninov@gmail.com*

Received January 29, 2024; revised February 19, 2024; accepted February 21, 2024

Abstract—New tin(IV) complexes $(L^n)SnR_2$ (R = *n*-Bu (**I**, **II**), *t*-Bu (**III**–**V**), and Ph (**VI**)) with O,N,O'-donor Schiff bases are synthesized. The molecular structures of compounds **I** and **IV** in the crystalline state are determined by XRD (CIF files CCDC nos. 2309864 (**I**) and 2309422 (**IV**)). The photophysical properties of the complexes are studied in comparison with the previously synthesized compounds containing phenyl or ethyl hydrocarbon groups at the tin atom. All compounds luminesce in chloroform: the emission bands are observed in the range from 580 to 638 nm. Both the groups at the tin atom and nature of the substituents in Schiff bases significantly affect the relative quantum yield. The anti/prooxidant activity of $(L^n)SnR_2$ in the reactions with the ABTS (2,2'-azinobis(3-ethylbenzothiazoline-6-sulfonic acid)) radical cation and superoxide radical anion, in the oxidative DNA damage, and during lipid peroxidation in vitro is studied. A weak antibacterial activity against the bacterial strains *Staphylococcus aureus* ANCC 6538 and *E. faecium* ATCC 3576 are observed for some compounds. The in vitro antiproliferative properties for a number of the complexes are studied for the HTC-116 and A-549 cancer cell lines. The coordination of the organometallic fragment with the O,N,O'-tridentate ligands is found to induce a pronounced decrease in the cytotoxicity of the complexes.

Keywords: tin(IV) complexes, tridentate Schiff bases, luminescence, antioxidant activity, cytotoxicity

DOI: 10.1134/S1070328424600293

INTRODUCTION

Tin(II/IV) complexes with redox-active ligands attract researchers' attention due to many valent states caused by the ability of the ligands to change the oxidation state. Similar complexes have a broad set of redox forms generated under electrochemical conditions or under the action of chemical reagents [1–6] and can actively participate in redox transformations [7], initiate the C–Hal bond cleavage and C–C bond formation [8, 9], and provide the charge transfer in the heteroligand compounds [10]. A phenomenon of redox isomerism of the Main Group metal has first been found for the tin complex with *o*-amidophenolate ligands [11]. In the field of synthesis of new biologically active organometallic coordination tin compounds, progress is observed in the preparation of substances containing privileged heterocyclic scaffolds, diverse redox-active fragments, and other pharmacophoric functional groups due to their high antiproliferative and antitumor activity [12–15].

Polydentate Schiff bases bearing redox-active fragments also play an important role in coordination chemistry, since they can form stable chelates with a wide range of metals. The tin(IV) derivatives are not exceptions and are intensively studied owing to unusual photophysical properties [16], which find use in the development of related materials for optoelectronic devices [17, 18] and solar batteries [19, 20]. The tin complexes with Schiff bases are luminescent and, hence, are considered as potential agents for bioimaging [21–23].

Along with specific optical properties, the tin(IV) complexes with Schiff bases are inherent in antimicrobial, antiproliferative, and antitumor activities [24–26]. Their high toxicity prevents the development of new tin-containing therapeutic agents. One of the solutions of this problem is a rational design of ligands:

the introduction of various antioxidant cytoprotector groups, which favors an enhancement of selectivity toward healthy cells and a decrease in side effects [27–29]. The variation of hydrocarbon groups at the tin atom and heteroatoms (O,N,S) involved in the formation of the coordination mode and the presence of additional redox-active fragments in the ligand structure make it possible to modulate the biological properties of the tin(IV) complexes in a wide range.

The purpose of this work is the synthesis of new tin(IV) complexes with O,N,O'-donor Schiff bases, study their structures, and analysis of the photophysical properties, anti- or prooxidant activity, and cytotoxicity in comparison with the previously synthesized related complexes to determine the influence of the substituents at the tin atom or in the ligands on the manifested properties.

EXPERIMENTAL

Commercial reagents Ph_2SnCl_2 (Aldrich, 96%), *n*-Bu_2SnCl_2 (Aldrich, 98%), *t*-Bu_2SnCl_2 (Aldrich, 96%), 2,2'-azobis(2-amidinopropane) dihydrochloride (AAPH) (97%, Aldrich), 2,2'-azinobis(3-ethylbenzothiazoline-6-sulfonic acid) (ABTS) (≥98%, TCI, Tokyo, Japan), thiobarbituric acid (≥98%, Sigma-Aldrich), deoxyribonucleic acid (DNA) sodium salt from salmon testes (Sigma), ethylenediaminotetraacetic acid (EDTA) (≥99%, Sigma-Aldrich), xanthine (3,7-dihydropurine-2,6-dione) (≥99%, Sigma-Aldrich), bovine serum albumin (≥96%, Sigma-Aldrich), xanthine oxidase (IV sort, Sigma-Aldrich), tetrasolium blue (90%, Alfa Aesar), phosphate buffer (pH 7.4, Sigma), 6-hydroxy-2,5,7,8-tetramethylchromane-2-carboxylic acid (Trolox) (97%, Aldrich), trichloroacetic acid (≥99%, Sigma-Aldrich), quinine sulfate dihydrate (TRC inc.), Dulbecco's Modified Eagle's Medium (DMEM medium, PanEko, Russia), Mueller–Hinton broth (MHB medium, PanEko, Russia), L-glutamine (PanEko, Russia), fetal bovine serum (Hyclone, Austria), ciprofloxacin (for biochemistry, AppliChem Biochemica Chemical Synthesis Services), penicillin (PanEko, Russia), streptomycin (PanEko, Russia) and 3-(4,5-dimethylthiazol-2-yl)-2,5-diphenyltetrazolium bromide (MTT, PanEko, Russia) were used as received. Schiff bases ((2,4-di-*tert*-butyl-6-((((5-*tert*-butyl)-2-hydroxyphenyl)imino)methyl)phenol (L^1H_2), 2,4-di-*tert*-butyl-6-(((5-chloro-2-hydroxy-3-nitrophenyl)-imino)methyl)phenol (L^2H_2), 2,4-dichloro-6-((3,5-di-*tert*-butyl-2-hydroxybenzilydene)amino)-3-methylphenol (L^3H_2), and 2,4-di-*tert*-butyl-6-((3,5-di-*tert*-butyl-2-hydroxybenzilydene)amino)phenol (L^4H_2)) were synthesized using a previously described procedure [30, 31]. The solvents used were purified and dehydrated using standard procedures [32].

^1H and ^{13}C NMR spectra were recorded on a Bruker AVANCE HD 400 spectrometer with frequencies of 400 (^1H) and 100 MHz (^{13}C) using $CDCl_3$ as the solvent. IR spectra were detected on an FSM 1201 FT-IR spectrometer in KBr pellets. High resolution mass spectra (HR-MS) were recorded on a Bruker UHR-TOF Maxis™ mass spectrometer in the electrospray ionization (ESI) regime. Electronic absorption spectra were measured on an SF-104 spectrophotometer in a range of 300–600 nm at room temperature. Fluorescence spectra were recorded on an SM-2203 spectrofluorimeter. Solutions of the complexes (c = 5 μmol/L) in $CHCl_3$ were used for recording fluorescence spectra at the excitation wavelength λ_{ex} = 340 nm. Relative fluorescence quantum yields (φ) were estimated in comparison with the standard: a 0.1 M solution of quinine sulfate in H_2SO_4 (φ = 0.577) [33]. The fluorescence of the target compounds was measured three times.

The initial compounds were dissolved in DMSO (0.001 mol/L) to study the stability of complexes **II**, **IV**, **IX**, and **X** in aqueous solutions at various pH. An aliquot of the starting solution of DMSO was introduced into an aqueous solution with the pH varied from 4 to 9, or a phosphate buffer with pH 7.4 was used. The final concentration of the complexes in the solutions was 5 μmol/L. To maintain a certain pH in the medium, 1 M solutions of HCl or KOH were used. The measurements were conducted in three repetitions.

The radical scavenging and antioxidant activity of the compounds in the reaction with the $ABTS^{\bullet+}$ radical cation was estimated using a known procedure [34]. The change in the absorption intensity of $ABTS^{\bullet+}$ (λ = 734 nm) generated under the action of $K_2S_2O_8$ was detected in the presence of the tin complexes in various concentrations (5–100 μmol/L). The value of IC_{50} was calculated as a minimum concentration of the compounds necessary to decrease the $ABTS^{\bullet+}$ content by 50% of the initial parameter. The plots of the dependences of the absorbance on the concentration in the ABTS test were constructed for the studied complex and Trolox. The antioxidant capacity ($ABTS_{TEAC}$) in the Trolox equivalents (Trolox equivalent antioxidant capacity, TEAC) was measured by comparing the slope angle of the plots for each compound with the data for Trolox.

The xanthine–xanthine oxidase enzymatic system (NBT test) was used for the estimation of the antiradical activity of the tin complexes toward $O_2^{\bullet-}$ [35]. The change in the absorbance at λ = 560 nm in the presence of the complexes in DMSO was monitored on a Thermo Scientific Multiskan Sky microplate spectrophotometer for 800 s. The control experiment was conducted by the replacement of a solution of the sample by the same amount of DMSO. The value of inhibition I (%) was calculated by the following equation: I (%) = $[(1 - A_i/A_0) \times 100\%]$, where A_i is the absorbance upon the addition of the target com-

pounds after incubation for 800 s, and A_0 is the absorbance of the control solution. The values of IC_{50} were determined graphically using the dependence of the inhibition percentage on the compound concentration, which was varied from 5 to 100 μmol/L. All experiments were carried out three times.

The Wistar rat liver homogenates (1 : 10 wt/vol) were prepared directly before use in a phosphate buffer medium (pH 7.4) using a homogenizer. The intensity of the lipid peroxidation (LP) of the liver homogenates was estimated from the accumulation of carbonyl products that formed a colored complex with thiobarbituric acid (TBARS) according to a previously described procedure [36]. The concentration of the tin complexes was 0.1 mmol/L. The TBARS concentration was determined after 3, 24, and 48 h of incubation at 37°C. The oxidative DNA damage in the presence of the AAPH radical initiator (37°C) and studied compounds (50 μmol/L) was evaluated according to a previously described procedure [37].

The minimum inhibitory concentration (MIC) was determined by the method of twofold serial dilutions according to the CLSI protocols [38]. The bacterial strains *Staphylococcus aureus* ATCC 6538, *Escherichia coli* ATCC 25922, and *Enterococcus faecium* ATCC 3576 from the American Type Culture Collection (ATCC, USA) were used. The Mueller–Hinton broth served as the nutrient medium for bacteria. The compounds were introduced into wells of the plate as DMSO solutions. The studied compounds were dissolved in DMSO and diluted with the MHB. The DMSO content in the studied solution did not exceed 12% and exerted no effect on the bacterial growth. The concentration of bacteria in the plate wells was 5×10^5 CFU/mL. All experiments were conducted in three analytical and two biological repetitions. Ciprofloxacin and levofloxacin served as positive controls.

The cytotoxicity of complexes **VI**, **VIII**, **IX**, **X**, and **XII** was determined in vitro on the lung cancer (A-549) and colorectal cancer (HCT-116) cell lines from the ATCC (Manassas, Virginia, USA). The cells were cultivated in the DMEM nutrient medium with the addition of 10% fetal bovine serum, L-glutamine (2 mmol/L), 1% penicillin, and 1% streptomycin at 37°C and 5% CO_2. The studied complexes were dissolved in DMSO to have an initial concentration of 10 mmol/L followed by serial dilutions in the cultural medium. The final concentration of DMSO was lower than 0.1% and exerted no effect on the cell viability. The cell viability after the action of the studied compounds was determined by the MTT test. The cells (5×10^3 in 190 μL of the cultural medium) were seeded in 96-well plates for 24 h and treated with the tin complexes in concentrations of 0.10–150.00 μmol/L for 72 h. After the treatment with the studied compounds, the MTT reagent (10 μL, 5.00 mg/mL) was added to each well for 1 h. After incubation, the nutrient medium was removed, DMSO (200 μL) was added, and the absorbance at $\lambda = 540$ nm was measured. The values of IC_{50} were calculated as the concentration of the compound necessary for decreasing the cell viability by 50% compared to the control cell growth (100%). Every assay was conducted in three samples in two independent experiments. The negative control in the MTT test was DMSO in a concentration of 0.1%, and doxorubicin hydrochloride served as the positive control.

Synthesis of tin complexes (L)SnR_2 (I–VI) was conducted by the exchange reaction of R_2SnCl_2 (0.3 mmol) with Schiff base L^1H_2–L^4H_2 (1 equiv) in acetonitrile in the presence of triethylamine (2 equiv) using a previously described procedure [30].

Complex (L^1)Sn^{n}Bu$_2$ (**I**). The yield of complex **I** as brightly orange crystals was 46% (0.085 g). IR (KBr; ν, cm^{-1}): 3061, 2033, 2995, 2958, 2921, 2871, 1611, 1589, 1557, 1544, 1528, 1500, 1488, 1457, 1430, 1385, 1362, 1330, 1294, 1279, 1253, 1230, 1197, 1168, 1129, 1087, 1023.

^{1}H NMR (400 MHz; $CDCl_3$; δ, ppm): 0.83 (t, ^3J(H,H) = 7.3 Hz, 6H, CH_3 from *n*-Bu), 1.29 (q, ^3J(H,H) = 7.3 Hz, 4H, CH_2 from *n*-Bu), 1.33 (s, 9H, *t*-Bu), 1.35 (s, 9H, *t*-Bu), 1.41 (s, 9H, *t*-Bu), 1.41–1.47 (m, 4H, CH_2 from *n*-Bu), 1.61–1.70 (m, 4H, CH_2 from *n*-Bu), 6.80 (d, ^3J(H,H) = 8.6 Hz, 1H, arom. C_6H_3), 7.06 (d, ^4J(H,H) = 2.5 Hz, 1H, arom. C_6H_2), 7.22 (dd, ^3J(H,H) = 8.6 Hz, ^4J(H,H) = 2.3 Hz, 1H, arom. C_6H_3), 7.31 (d, ^4J(H,H) = 2.3 Hz, 1H, arom. C_6H_3), 7.50 (d, ^4J(H,H) = 2.5 Hz, 1H, arom. C_6H_2), 8.64 (s, ^3J(H,Sn) = 50.6 Hz, 1H, CH=N).

^{13}C NMR (100 MHz, $CDCl_3$, δ, ppm): 13.52, 21.87 (^1J(C,Sn) = 622, 595 Hz), 26.74 (^2J(C,Sn) = 90.6 Hz), 26.95 (^3J(C,Sn) = 32.4 Hz), 29.38, 31.27, 31.66, 34.04, 34.28, 35.21, 111.01, 117.06, 117.58, 126.74, 128.93, 130.81, 131.73, 138.16, 138.99, 140.91, 157.00, 161.84, 167.37.

HR-MS: Found *m/z*: 614.2998 $[M + H]^+$. $C_{33}H_{52}NO_2Sn$. Calculated *m/z*: 614.3021.

Complex (L^2)Sn^{t}Bu$_2$ (**II**). The yield of complex **II** as a dark red powder was 84% (0.160 g). IR (KBr; ν, cm^{-1}): 3086, 2964, 2849, 1611, 1588, 1555, 1532, 1517, 1464, 1418, 1406, 1388, 1363, 1349, 1256, 1228, 1200, 1167, 1134, 1028, 1015.

^{1}H NMR (400 MHz; $CDCl_3$; δ, ppm): 0.83 (t, ^3J(H,H) = 7.3 Hz, 6H, CH_3 from *n*-Bu), 1.22–1.35 (m, 4H, CH_2 from *n*-Bu), 1.31 (s, 9H, *t*-Bu), 1.39 (s, 9H, *t*-Bu), 1.50–1.70 (m, 8H, CH_2 from *n*-Bu), 7.05 (d, ^4J(H,H) = 2.5 Hz, 1H, arom. C_6H_2), 7.45 (d, ^4J(H,H) = 2.5 Hz, 1H, arom. C_6H_2), 7.59 (d, ^4J(H,H) = 2.5 Hz, 1H, arom. C_6H_2), 7.87 (d, ^4J(H,H) = 2.5 Hz, 1H, arom. C_6H_2), 8.59 (s, with sat-

ellite splitting on tin nuclei ^3J(H,Sn) = 43.7 Hz, 1H, CH=N).

^{13}C NMR (100 MHz, $CDCl_3$, δ, ppm): 13.46, 22.59 (^1J(C,Sn) = 606, 577 Hz), 26.57 (^2J(C,Sn) = 90.6 Hz), 26.72 (^3J(C,Sn) = 36 Hz), 29.32, 31.05, 34.08, 35.23, 116.90, 118.50, 119.50, 124.29, 129.49, 134.21, 136.91, 138.01, 139.41, 141.55, 154.28, 164.70, 168.98.

HR-MS: Found *m/z*: 659.1678 $[M + Na]^+$. $C_{29}H_{41}ClN_2NaO_4Sn$. Calculated *m/z*: 659.1668.

Complex $(L^1)Sn^tBu_2$ (**III**). The yield of complex **III** as a red powder was 57% (0.105 g). IR (KBr; ν, cm^{-1}): 3067, 3051, 2958, 2878, 2583, 1610, 1588, 1557, 1530, 1497, 1487, 1467, 1458, 1427, 1406, 1380, 1362, 1315, 1297, 1280, 1252, 1232, 1198, 1169, 1138, 1128, 1027.

^{1}H NMR (400 MHz; $CDCl_3$; δ, ppm): 1.33 (s, 27H, *t*-Bu), 1.34 (s, 9H, *t*-Bu), 1.46 (s, 9H, *t*-Bu), 6.82 (d, ^3J(H,H) = 8.5 Hz, 1H, arom. C_6H_3), 7.06 (d, ^4J(H,H) = 2.6 Hz, 1H, arom. C_6H_2), 7.20 (dd, ^3J(H,H) = 8.6 Hz, ^4J(H,H) = 2.3 Hz, 1H, arom. C_6H_3), 7.24 (d, ^4J(H,H) = 2.3 Hz, 1H, arom. C_6H_3), 7.51 (d, ^4J(H,H) = 2.6 Hz, 1H, arom. C_6H_2), 8.67 (s, with satellite splitting on tin nuclei ^3J(H,Sn) = 46.9 Hz, 1H, CH=N).

^{13}C NMR (100 MHz; $CDCl_3$; δ, ppm): 29.81, 30.30, 31.26, 31.68, 34.00, 34.23, 35.40, 40.47 (*J*(C,Sn) = 605, 582 Hz), 111.18, 117.20, 117.60, 126.56, 129.10, 131.54, 131.82, 137.97, 138.39, 140.61, 157.74, 161.80, 168.87.

HR-MS: Found *m/z:* 614.2950 $[M + H]^+$. $C_{33}H_{52}NO_2Sn$. Calculated *m/z:* 614.2952.

Complex $(L^2)Sn^tBu_2$ (**IV**). The yield of complex **IV** as brick-red crystals was 82% (0.156 g). IR (KBr; ν, cm^{-1}): 3085, 2963, 2871, 2852, 1610, 1589, 1555, 1532, 1517, 1464, 1418, 1406, 1389, 1363, 1348, 1317, 1258, 1225, 1200, 1170, 1135, 1029, 1015.

^{1}H NMR (400 MHz; $CDCl_3$; δ, ppm): 1.31 (s, 9H, *t*-Bu), 1.34 (s, 18H, *t*-Bu), 1.44 (s, 9H, *t*-Bu), 7.04 (d, ^4J(H,H) = 2.6 Hz, 1H, arom. C_6H_2), 7.38 (d, ^4J(H,H) = 2.5 Hz, 1H, arom. C_6H_2), 7.61 (d, ^4J(H,H) = 2.6 Hz, 1H, arom. C_6H_2), 7.86 (d, ^4J(H,H) = 2.5 Hz, 1H, arom. C_6H_2), 8.62 (s, with satellite splitting on tin nuclei ^3J(H,Sn) = 39.4 Hz, 1H, CH=N).

^{13}C NMR (100 MHz, $CDCl_3$, δ, ppm): 29.72, 30.08, 31.05, 34.06, 35.42, 41.81, 117.39, 118.01, 119.32, 124.13, 129.66, 134.29, 137.56, 137.77, 139.31, 141.33, 154.64, 164.76, 170.26.

HR-MS: Found *m/z*: 659.1650 $[M + Na]^+$. $C_{29}H_{41}ClN_2NaO_4Sn$. Calculated *m/z*: 659.1668.

Complex $(L^3)Sn^tBu_2$ (**V**). The yield of complex **V** as an orange powder was 74% (0.141 g). IR (KBr; ν, cm^{-1}): 3067, 2955, 2927, 2871, 1609, 1589, 1552, 1531, 1507, 1454, 1428, 1405, 1387, 1361, 1317, 1303, 1265, 1251, 1232, 1198, 1179, 1136, 1072, 1050.

^{1}H NMR (400 MHz; $CDCl_3$; δ, ppm): 1.31 (s, 9H, *t*-Bu), 1.34 (s, 18H, *t*-Bu), 1.45 (s, 9H, *t*-Bu), 2.45 (s, 3H, CH_3), 7.02 (d, ^4J(H,H) = 2.6 Hz, 1H, arom. C_6H_2), 7.21 (s, 1H, arom. C_6H_1), 7.55 (d, ^4J(H,H) = 2.6 Hz, 1H, arom. C_6H_2), 8.60 (s, with satellite splitting on tin nuclei J(H,Sn) = 43.2 Hz, 1H, CH=N).

^{13}C NMR (100 MHz; $CDCl_3$; δ, ppm): 17.86, 29.79, 30.15, 31.15, 33.99, 35.39, 41.06 (^1J(C,Sn) = 573 Hz), 112.96, 117.36, 120.09, 123.84, 129.34, 131.08, 132.79, 134.13, 138.49, 140.89, 155.02, 162.78, 169.27.

HR-MS: Found *m/z*: 640.1700 $[M + H]^+$. $C_{30}H_{44}Cl_2NO_2Sn$. Calculated *m/z*: 640.1759.

Complex $(L^3)SnPh_2$ (**VI**). The yield of complex **V** as an orange-red powder was 86% (0.175 g). IR (KBr; ν, cm^{-1}): 3051, 2958, 2909, 2868, 1608, 1595, 1554, 1531, 1506, 1450, 1430, 1388, 1361, 1302, 1272, 1251, 1230, 1198, 1180, 1135, 1073, 1025.

^{1}H NMR (400 MHz, $CDCl_3$, δ, ppm): 1.33 (s, 9H, *t*-Bu), 1.55 (s, 9H, *t*-Bu), 2.49 (s, 3H, CH_3), 7.08 (d, ^4J(H,H) = 2.5 Hz, 1H, arom. C_6H_2), 7.29 (s, 1H, arom. C_6H_1), 7.34–7.47 (m, 6H, Ph), 7.65 (d, ^4J(H,H) = 2.5 Hz, 1H, arom. C_6H_2), 7.87–7.95 (m, with satellite splitting on tin nuclei J(H,Sn) = 80.8 Hz, 4H, Ph), 8.65 (s, with satellite splitting on tin nuclei J(H,Sn) = 59.2 Hz, 1H, CH=N).

^{13}C NMR (100 MHz, $CDCl_3$, δ, ppm): 17.92, 29.91, 31.13, 34.06, 35.48, 113.03, 117.07, 121.41, 124.45, 128.71 (*J*(C,Sn) = 88 Hz), 129.82, 130.09, 130.34 (*J*(C,Sn) = 17 Hz), 133.48, 134.78, 136.39 (*J*(C,Sn) = 56 Hz), 139.43, 139.53, 141.15, 153.70, 163.21, 167.98.

HR-MS: Found *m/z*: 680.1099 $[M + H]^+$. $C_{34}H_{36}Cl_2NO_2Sn$. Calculated *m/z*: 680.1134.

Complexes $(L^1)SnPh_2$ (**VII**), $(L^1)SnEt_2$ (**VIII**), $(L^2)SnPh_2$ (**IX**), $(L^2)SnEt_2$ (**X**), $(L^3)SnEt_2$ (**XI**), $(L^4)SnPh_2$ (**XII**), and $(L^4)SnEt_2$ (**XIII**) were synthesized using a previously published procedure [30].

XRD. The crystals of complex **I** suitable for XRD were prepared by the slow evaporation of its solution in acetonitrile at room temperature. A set of experimental data was collected on an Agilent SuperNova diffractometer using a microfocus X-ray radiation source with a copper anode and an Atlas S2 CCD coordinate detector. Data were collected and unit cell parameters were determined and refined using the CrysAlisPro 1.171.38.41 specialized software [39]. The diffraction data on the crystals of compound **IV** were collected on a D8 Venture single-crystal X-ray diffractometer (ω scan mode, MoK_α radiation, λ = 0.71073 Å). For experimental data processing, a semiempirical absorp-

Table 1. Crystallographic data and structure refinement details for compounds **I** and **IV**

Complex	**I**	**IV**
Empirical formula	$C_{66}H_{102}N_2O_4Sn_2$	$C_{29}H_{41}N_2O_4ClSn$
FW	1224.87	635.78
T, K	293(2)	220(2)
Source	CuK_α	MoK_α
Wavelength, Å	1.54184	0.71073
Crystal system	Monoclinic	Triclinic
Space group	$P2_1/n$	$P\bar{1}$
a, Å	12.44580(10)	13.7848(6)
b, Å	9.61530(10)	13.9371(6)
c, Å	27.0296(3)	18.2814(7)
α, deg	90	68.0398(14)
β, deg	102.9510(10)	84.2036(14)
γ, deg	90	71.8718(14)
V, Å^3	3152.35(6)	3095.2(2)
Z	2	4
ρ_{calc}, mg/m^3	1.290	1.364
μ, mm^{-1}	6.647	0.945
θ, deg	3.654–76.478	1.902–28.000
Number of measured/independent reflections	33544/6595	54203/14 954
Number of independent reflections with $I > 2\sigma(I)$	6384	11880
R_{int}	0.0395	0.0304
GOOF (F^2)	1.058	1.025
R_1, wR_2 ($I > 2\sigma(I)$)	0.0304, 0.0821	0.0290, 0.0590
R_1, wR_2 (for all parameters)	0.0313, 0.0830	0.0434, 0.0640
$\Delta\rho_{max}/\Delta\rho_{min}$, e Å^{-3}	1.538/–1.243	0.450/–0.448

tion correction was applied using the SADABS program [40]. The structure was solved by direct methods and refined by full-matrix least squares for F^2 in the anisotropic approximation for all non-hydrogen atoms. Hydrogen atoms were placed in the calculated positions and refined by the riding model with $U_{iso}(H) = 1.5U_{eq}(C)$ in the methyl groups and $U_{iso}(H) = 1.2U_{eq}(C)$ in other fragments. The calculations were performed using the SHELXL software [41]. The crystallographic data and structure refinement parameters for compounds **I** and **IV** are given in Table 1.

The crystallographic parameters were deposited with the Cambridge Crystallographic Data Centre (CIF files CCDC nos. 2309864 (**I**) and 2309422 (**IV**); deposit@ccdc.cam.ac.uk; http://www.ccdc.cam.ac.uk).

The quantum chemical modeling of isolated molecules of compounds **VIII**–**XIII** was performed using the Gaussian09 (D01) program [42]. The geometry of each molecule was optimized at the PBE0-D3/def2TZVP level [43–45] using standard convergence criteria and taking into account nonspecific solvation in the framework of the polarization continuum model (dielectric constant of chloroform) [46]. The root-mean-square deviation of the calculated positions of non-hydrogen atoms from those obtained from the XRD data was at most 0.1 Å. According to the normal vibration analysis performed at the same level of the theory, all determined structures correspond to

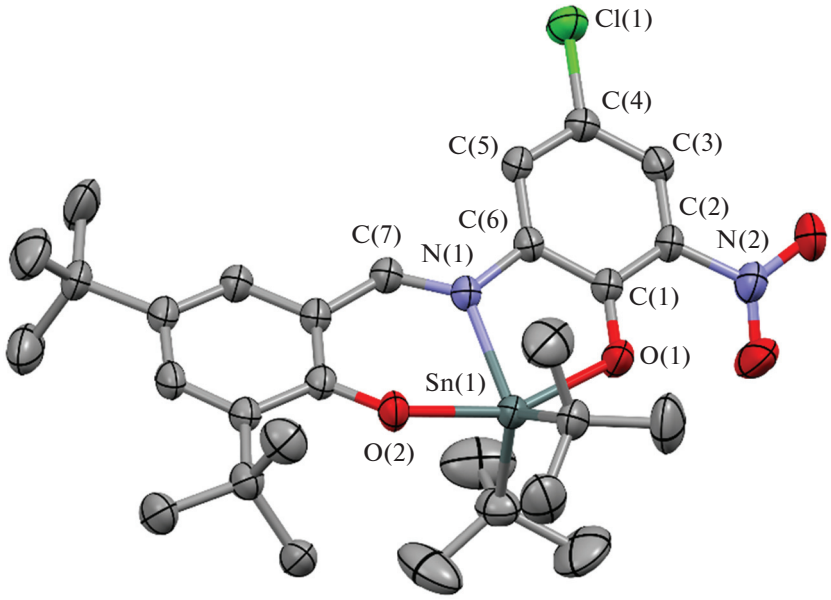

Fig. 1. Molecular structure of complex $L^2Sn^tBu_2$ (**IV**) according to the XRD data. Hydrogen atoms are omitted. Ellipsoids of 50% probability.

minima on the potential surface energy. Excited states were simulated in the framework of the time-dependent density functional theory (DFT), and the basis set was selected for compound **VIII** from the resource intensity ratio and coincidence with experimental data on absorption bands in the UV spectra. Further the spectral data for all the six compounds were calculated using the def2TZVP basis set at three DFT levels (B3LYP, PBE0, CAM-B3LYP). The excited states were additionally calculated for the B3LYP/def2TZVP level taking into account the solvation polarization continuum model (dielectric constant of chloroform).

RESULTS AND DISCUSSION

Tin complexes $LSnR'_2$ (**I**–**VI**) were formed due to the exchange reactions of Schiff bases (L^1H_2–L^4H_2) and R'_2SnCl_2 in a ratio of 1 : 1 in acetonitrile in the presence of triethylamine as the deprotonating agent (Scheme 1). Compounds **VII**–**XIII** were synthesized previously by a similar procedure [30].

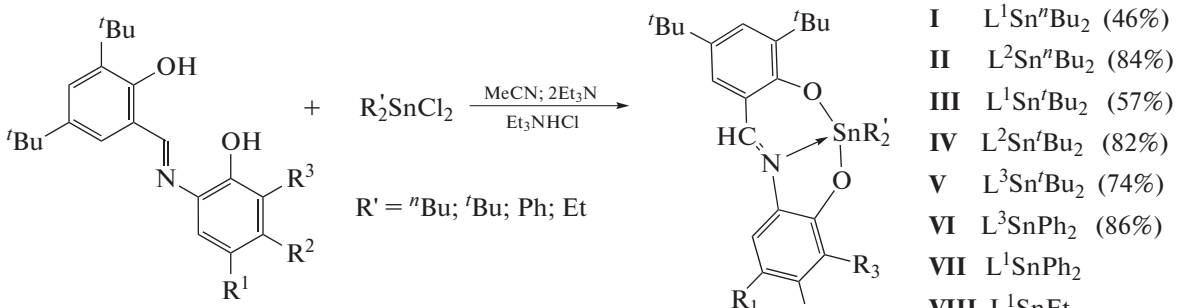

L^1H_2 $R^1 = R^2 = H$; $R^3 = {}^t$Bu;
L^2H_2 R^1 = Cl; $R^2 = H$; $R^3 = NO_2$;
L^3H_2 $R^1 = R^3$ = Cl; R^2 = Me;
L^4H_2 $R^1 = R^3 = {}^t$Bu; $R^2 = H$

I $L^1Sn^nBu_2$ (46%)
II $L^2Sn^nBu_2$ (84%)
III $L^1Sn^tBu_2$ (57%)
IV $L^2Sn^tBu_2$ (82%)
V $L^3Sn^tBu_2$ (74%)
VI L^3SnPh_2 (86%)
VII L^1SnPh_2
VIII L^1SnEt_2
IX L^2SnPh_2
X L^2SnEt_2
XI L^3SnEt_2
XII L^4SnPh_2
XIII L^4SnEt_2

Scheme 1.

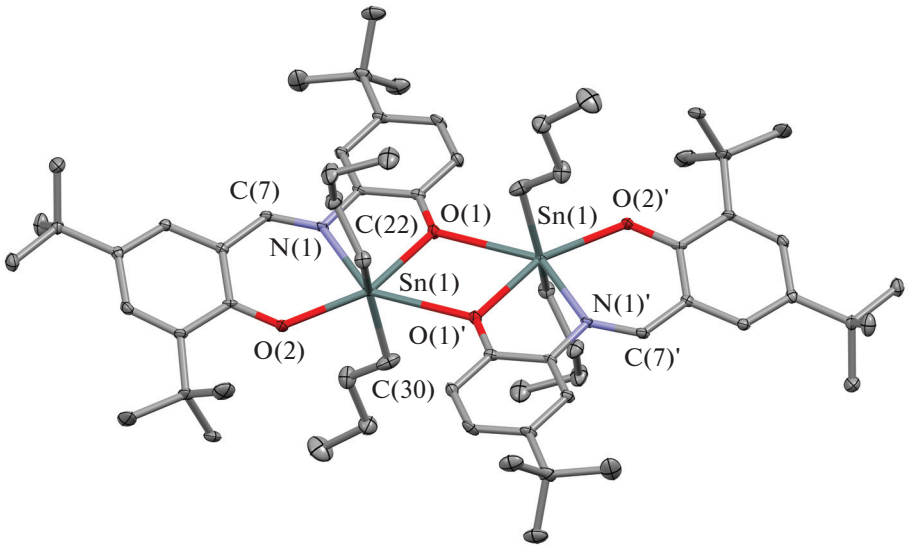

Fig. 2. Molecular structure of complex $L^1Sn^nBu_2$ (**I**) according to the XRD data. Hydrogen atoms are omitted. Ellipsoids of 50% probability.

Complexes **I**–**VI** were isolated by filtration as orange-red crystalline powders in the yields up to 86%. The compositions and structures of compounds **I**–**VI** were determined by the data of IR and ^1H and ^{13}C NMR spectroscopy and high resolution mass spectrometry. The molecular structures of complexes $L^1Sn^nBu_2$ (**I**) and $L^2Sn^tBu_2$ (**IV**) in the crystalline state were determined by XRD (Figs. 1, 2). Selected bond lengths and angles are listed in Table 2.

Complex $L^2Sn^tBu_2$ (**IV**) is the mononuclear derivative of pentacoordinated tin(IV) with the O,N,O'-tridentate redox-active ligand. On the whole, the structure of this complex in crystal is close to those of the earlier studied tin(IV) complexes $(ONO)SnR_2$ and $(ONS)SnR_2$ [19, 47–53]. On the contrary, complex $L^1Sn^nBu_2$ (**I**), which is also mononuclear according to the solution NMR data, represents dimer $[L^1Sn^nBu_2]_2$ in the crystalline state (Fig. 2). A similar structure was shown for the related tin complexes, for instance, $Et_2Sn(t\text{-}Bu_2ONO{-}Cl_2{-}Me)$ [30] and $n\text{-}Bu_2Sn(Cl_2ONO{-}NO_2)$ [50].

The geometric characteristics of the redox-active ligand in the complexes are characteristic of iminobis(phenolates). The C–O bond lengths (1.302(3) and 1.317(3) Å in **IV**; 1.338(2) and 1.307(2) Å in **I**) lie in the range of these bonds characteristic of various tin phenolates. The six-membered carbon rings are aromatic (average C–C bond lengths in the $C_6O(2)C(7)$ and $C_6O(1)N(1)$ fragments are 1.403 and 1.391 Å in **IV**; 1.407 and 1.396 Å in **I**), and the C=N bond is double (1.312(3) and 1.302(2) Å, respectively). In the related $t\text{-}Bu_2Sn(MeO{-}ONO{-}NO_2)$ complexes, the C–O distances are 1.310 and 1.305 Å (average C–C 1.401 and 1.394 Å; C=N 1.310 Å). The C–O distances in $t\text{-}Bu_2Sn(ONO\text{-}NO_2)$ are 1.307 and 1.315 Å (average C–C 1.393 and 1.390 Å), and the C=N bond lengths are 1.307 Å [54]. In similar diphenyltin(IV) complexes, the C–O bond lengths vary in a range of 1.31–1.34 Å in the iminophenolate fragment $C_6O(1)N(1)$ and 1.30–1.32 Å in the phenolate fragment $C_6O(2)C(7)$ (C=N bond length ranges from 1.29 to

Table 2. Selected bond lengths (Å) and bond angles (deg) in complexes **I** and **IV**

Bond	**I***	**IV**
	d, Å	
Sn(1)–O(1)	2.141(1)	2.132(2)
Sn(1)–O(2)	2.179(2)	2.101(2)
Sn(1)–N(1)	2.208(1)	2.192(2)
Sn(1)–C(22)	2.127(2)	2.170(2)
Sn(1) –C(26)		2.170(3)
Sn(1)–C(30)	2.124(2)	
Angle	ω, deg	
O(1)Sn(1)O(2)	155.74(6)	155.68(7)
C(22)Sn(1)C(26)		129.6(1)
C(22)Sn(1)C(30)	147.27(8)	
N(1)Sn(1)C(22)	104.69(6)	122.18(8)
N(1)Sn(1)C(26)		107.87(9)
N(1)Sn(1)C(30)	106.95(7)	

* Sn(1)O(1'), 2.678(2) Å; O(1)Sn(1)O(1'), 65.90(5)°; O(2)Sn(1)O(1'), 38.36(5)°.

Table 3. Photophysical properties of complexes **I**–**XIII** in $CHCl_3$ at 293 K

Compound	λ_{max}^{abs}, nm ($\varepsilon \times 10^3$, mol L^{-1} cm^{-1})	ΔE, eV	λ_{ex}, nm	λ_{em}, nm	$\Delta\nu$, cm^{-1}	φ
$L^1Sn^nBu_2$ (**I**)	318 (6.85), 385 sh (4.04), 477 (13.46)	2.60	340	616	4731	0.375
$L^2Sn^nBu_2$ (**II**)	312 (8.48), 396 sh (6.17), 420 (8.06), 491 (17.93)	2.52	340	562 580	2573 3125	0.197
$L^1Sn^tBu_2$ (**III**)	310 (12.51), 396 sh (6.81), 480 (21.96)	2.58	340	612	4494	0.341
$L^2Sn^tBu_2$ (**IV**)	310 (9.16), 396 sh (5.10), 422 (7.56), 494 (16.88)	2.51	340	562 580	2449 3001	0.232
$L^3Sn^tBu_2$ (**V**)	319 (14.47), 393 sh (9.09), 485 (27.60)	2.56	340	594	3783	0.351
L^3SnPh_2 (**VI**)	320 (12.50), 394 (6.90), 473 (15.08)	2.62	340	582	3959	0.462
L^1SnPh_2 (**VII***)	324 (8.26), 390 sh (5.42), 473 (14.80)	2.62	340	610	4748	0.334
L^1SnEt_2 (**VIII***)	316 (7.51) 390 sh (5.51), 476 (15.61)	2.60	340	598	4286	0.357
L^2SnPh_2 (**IX***)	317 (8.52), 392 sh (5.56), 418 (8.82), 483 (17.24)	2.57	340	560 582	2846 3521	0.252
L^2SnEt_2 (**X***)	313 (7.95), 393 sh (5.66), 420 (7.93), 493 (17.58)	2.52	340	600	3334	0.180
L^3SnEt_2 (**XI***)	328 (6.98), 394 sh (5.34), 482 (17.57)	2.57	340	584	3623	0.415
L^4SnPh_2 (**XII***)	321 (18.80) 393 sh (5.81), 477 (16.51)	2.60	340	638	5291	0.129
L^4SnEt_2 (**XIII***)	328 (6.99), 394 sh (5.29), 481 (15.51)	2.57	340	638	5117	0.182

* The data on the electronic absorption spectra are taken from [30].

1.32 Å [30]). As already said, complex **I** in the crystalline state is dimer. In complex **I**, the coordination sphere of the Sn(1) tin atom is supplemented to the coordination number 6 due to the donor–acceptor interaction with the O(1) oxygen atom of the redox-active ligand (Sn(1)–O(1') distance 2.678(2) Å).

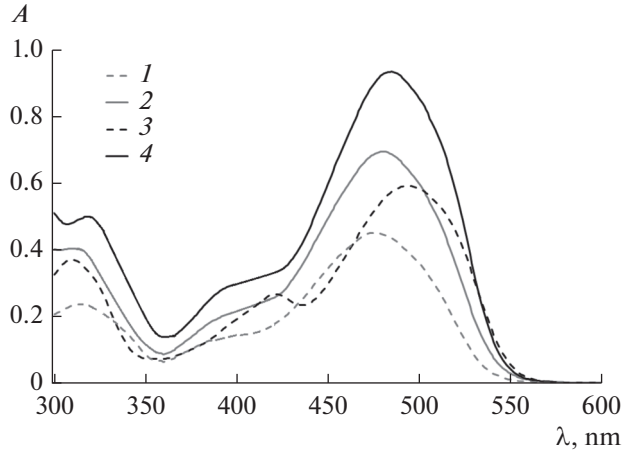

Fig. 3. Electronic absorption spectra of complexes (*1*) **I**, (*2*) **II**, (*3*) **IV**, and (*4*) (**V**) in $CHCl_3$ at 293 K (c = 3.0×10^{-5} mol/L).

The spectral properties of the synthesized complexes in the UV spectral range (300–600 nm) in chloroform were studied (Table 3).

The electronic absorption spectra of complexes **I**–**VI** (Fig. 3) differ insignificantly from the spectra detected earlier for compounds **VII**–**XIII** (Table 3). The spectra of complexes **I**, **III**, **V**, and **VI** exhibit two absorption bands and a shoulder at 385–396 nm. One of the absorption bands is attributed to the intramolecular charge transfer in the ligand (π–π* and *n*–π*), and the more intense band (473–493 nm) is related to the metal–ligand charge transfer [30]. For compounds **II** and **IV**, the presence of the chromophoric nitro group causes an additional intraligand *n*–π* charge transfer at 420 or 422 nm [21].

The substituents in the Schiff bases exert the highest effect on the position of the maximum in a range of 463–493 nm. Unlike the complexes with ligands L^1 and L^4 bearing donating *tert*-butyl groups, the introduction of electron-withdrawing substituents into L^2 favors the bathochromic shift of the most intense band by 10–17 nm. A similar behavior can be explained by the participation of the nitro group in the electron density redistribution in the conjugated system of the ligand. The substituents at the tin(IV) atom exert almost no effect on the position of the maximum, and only an insignificant hypsochromic effect is observed for the complexes with phenyl groups. In the case of

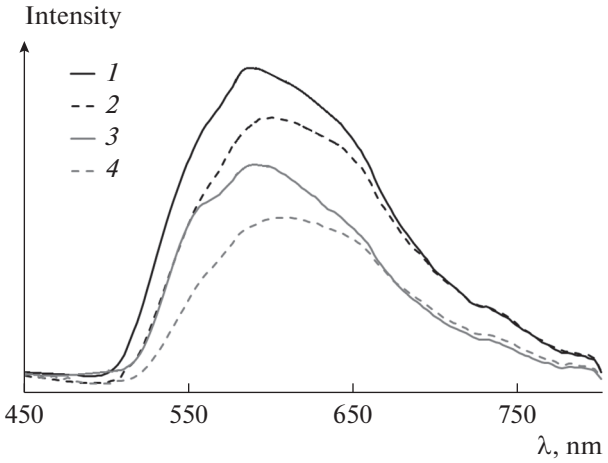

Fig. 4. Fluorescence spectra of complexes (*1*) **VI**, (*2*) **I**, (*3*) **V**, and (*4*) **IV** in $CHCl_3$ at 293 K ($c = 5.0 \times 10^{-6}$ mol/L).

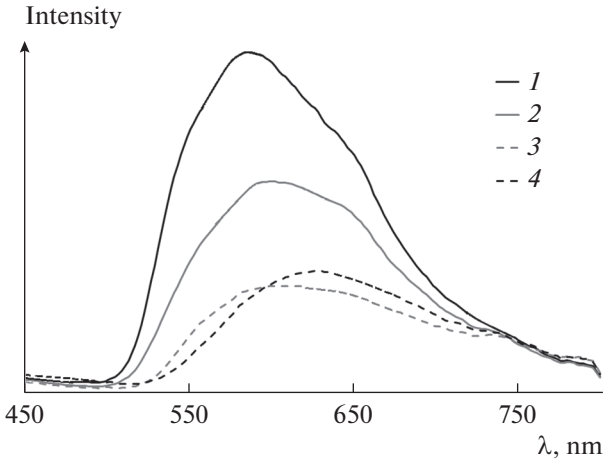

Fig. 5. Fluorescence spectra of complexes (*1*) **XI**, (*2*) **VIII**, (*3*) **X**, and (*4*) **XIII** in $CHCl_3$ at 293 K ($c = 5.0 \times 10^{-6}$ mol/L).

compounds **III** and **V**, the replacement of the *n*-butyl by *tert*-butyl substituents results in a considerable hyperchromic effect for the absorption band at 473–482 nm.

The study of the luminescence activity of complexes **I**–**XIII** (Table 3) shows one or two emission bands at $\lambda_{ex} = 340$ nm in the range from 560 to 638 nm (Fig. 4).

The relative quantum yield in the series of the complexes with Schiff base L^1 regularly decreases on going from the ethyl- to *n*-butyl-, *tert*-butyl-, and phenyl-substituted tin(IV) derivatives (Table 3). An inverse dependence is observed for the complexes with ligand L^2. The quantum yield for the compounds with the same alkyl groups at the tin atom depends on the nature of groups in the Schiff bases (Fig. 5).

The compounds can be arranged in the following order: $\varphi(R_2SnL^3) < \varphi(R_2SnL^1) < \varphi(R_2SnL^2) < \varphi(R_2SnL^4)$. The replacement of one of the chlorine atoms by the nitro group in L^2, as well as the introduction of the additional *tert*-butyl substituent in L^4, results in a decrease in the relative quantum yield. The maximum Stokes shifts were detected for the complexes with ligand L^4 containing donating *tert*-butyl groups. However, the compounds of this series are characterized by low quantum yields. The emission bands for the complexes with L^4 are observed at 610–638 nm, whereas λ_{em} was detected in a narrow range of 580–600 nm for the most part of the substances. Two peaks are observed in the emission spectra of the compounds with ligand L^2.

The energy gap (ΔE), being the difference in the energies of the frontier orbitals, is often used to evaluate the possibility of applying substances in photoelectric devices. This parameter predetermines the efficiency of solar radiation absorption [19] and the color of the light emitted in optoelectronic devices [55]. The value of ΔE can theoretically be determined using quantum chemical calculations or can be measured experimentally using UV-vis spectroscopy. The ΔE parameters for complexes **I**–**XIII** calculated from the spectral data are observed in the range from 2.51 to 2.62 eV and are close to the values obtained previously from the electrochemical experiments for complexes **VII**–**XIII** [30]. The minimum values of ΔE (2.51–

Table 4. Selected results of the quantum chemical B3LYP/def2TZVP calculations for compounds **VIII**–**XIII**

Compound	S_0 ΔE_{MO}	$S_0 \rightarrow S_1$ $\lambda^{abs}_{calc}/\lambda^{abs}_{exp}$	$S_0 \rightarrow S_1$ $\Delta E_{calc}/\Delta E_{exp}$	$S_0 \rightarrow S_2$ $\lambda^{abs}_{calc}/\lambda^{abs}_{exp}$	$S_0 \rightarrow S_3$ $\lambda^{abs}_{calc}/\lambda^{abs}_{exp}$
VIII	3.09	468/476	2.65/2.60	390/390	326/316
IX	3.18	465/483	2.66/2.57	407/418	387/392
X	3.11	475/493	2.61/2.52	410/420	391/393
XI	3.07	466/482	2.66/2.57	399/394	334/328
XII	3.12	468/477	2.65/2.60	394/393	336/321
XIII	3.09	477/471	2.60/2.57	396/394	337/328

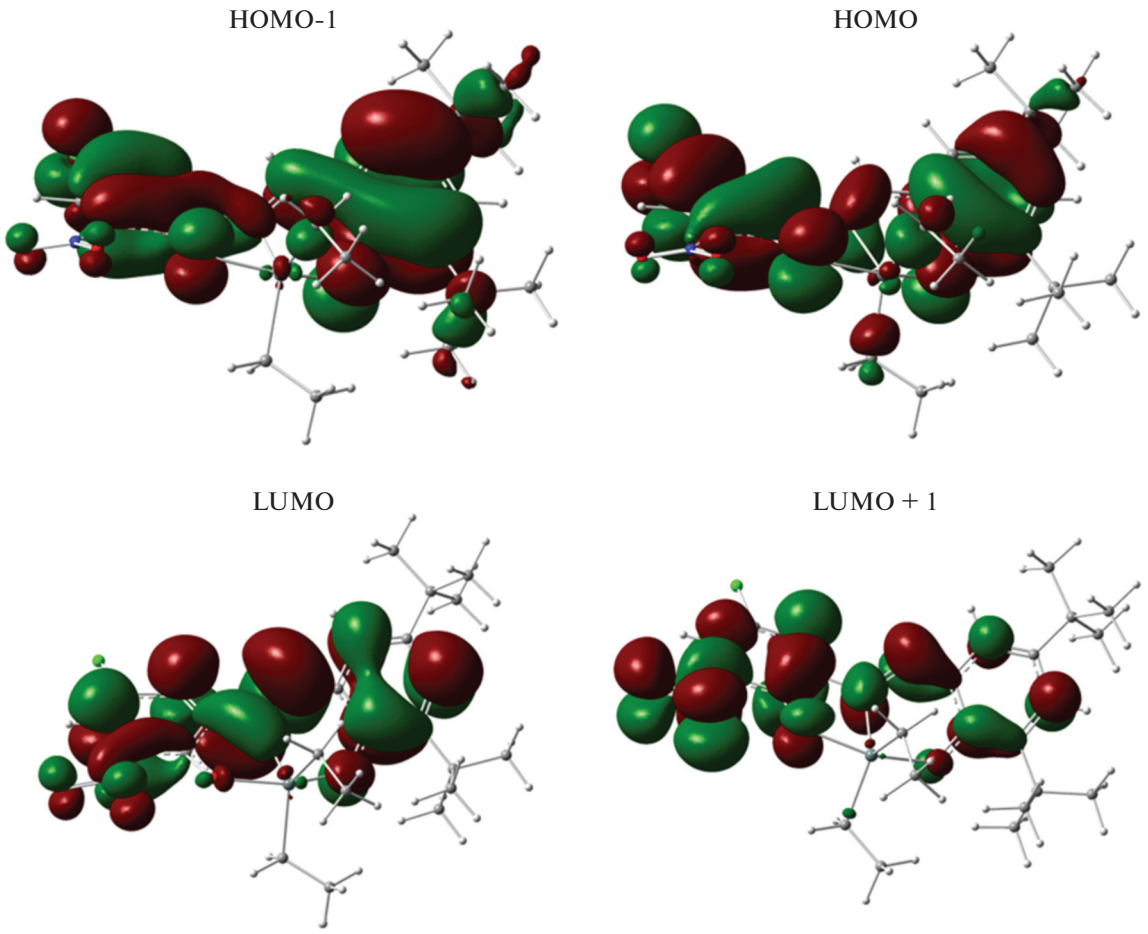

Fig. 6. Isosurfaces of the selected Kohn–Sham molecular orbitals (|0.02| au) calculated at the B3LYP/def2TZVP level for compound **X**.

2.52 eV) are characteristic of the complexes with alkyl groups linked to the tin atom and Schiff base L^2.

The quantum chemical calculations performed for compounds **VIII**–**XIII** are sufficiently consistent with the experimental data (Table 4). The wavelengths corresponding to the excitation energy $S_0 \rightarrow S_n$ (λ_{calc}^{abs}) calculated in the framework of the time-dependent DFT lie in narrow ranges of 465–477, 393–410, and 326–391 nm (for $n = 1$, 2, and 3, respectively), which is well consistent with the experimental values of λ_{exp}^{abs} and ΔE_{exp} estimated from them (Table 3). It is important that the calculated energy gap between the HOMO and LUMO (ΔE_{MO}) turns out to be substantially higher than the indicated values (average 3.11 eV) and does not correlate with either of them.

It is noteworthy that the best agreement of E_{exc} with the experiment is achieved for the B3LYP functional among the B3LYP, PBE0, and CAM-B3LYP methods, whereas two other methods and taking into account solvation effects in the polarization continuum model (IEFPCM, relative dielectric constant of chloroform) underestimate λ_{calc}^{abs} for the $S_0 \rightarrow S_1$ transition to a substantially higher extent. The effect of the basis set is insignificant: for compound **VIII**, the changes ΔE_{calc} are lower than 10 nm for the variation of the basis set (def2SVP, def2SVPP, def2TZVP, def2QZVP, aug-cc-pVTZ:28mdf, aug-cc-pVQZ:28mdf).

An analysis of populations of the Kohn–Sham molecular orbitals (isosurfaces of some of them are shown in Fig. 6) shows that the $S_0 \rightarrow S_1$ transitions in compounds **VIII**–**XIII** always correspond to the charge transfer between the HOMO and LUMO. The latter are localized mainly on the ligand and formally correspond to the π_b and π^* orbitals. It is important that the localization of both frontier boundaries in the vicinity of the metal atom is nearly the same and insignificant.

In all cases, the high-energy transition $S_0 \rightarrow S_2$ corresponds to the charge transfer from the HOMO-1, which is also localized on the ligand to a higher extent rather than on the HOMO. Finally, the $S_0 \rightarrow S_3$ transition is achieved due to either the charge transfer from

the HOMO-2 (localized on the ligand to a higher extent) to LUMO, or the transfer from the HOMO-1 to LUMO + 1 (localized on the ligand only). The observed distribution of the one-particle excitations is independent of the used calculation method.

The presence of the pH-sensitive nitro group in Schiff base L^2 capable of protonating evokes interest in the changes appeared in the visible spectral range for compounds **II**, **IV**, **IX**, and **X**. In addition, the stability of these complexes in aqueous solutions under the conditions of physiological pH can be estimated using absorption spectroscopy. The most intense absorption maximum in the visible range at 470–490 nm (pH 7) shifts to the long-wavelength range to 520 (**IX**), 505 (**X**), and 480 nm (**IV**) in an acidic medium (pH 4) for complexes **IV**, **IX**, and **X**. This indicates a possibility of the protonation of the nitro group (Fig. 7). Complex **II** is unstable under these conditions.

Complexes **IV** and **IX** turned out to be stable at pH 4–7 (Fig. 8). A decrease in the absorption maximum intensity at 480–485 nm was observed in an alkaline medium (pH 8). Complex **X** shows an inverse pattern: the absorption maximum intensity at 505 nm decreases at pH < 6.

The dynamics of changes in the spectra of the complexes in time at pH 7.0 and pH 7.4 in a phosphate buffer was considered. The nature of substituents at the tin atom exerts a substantial effect on the stability in time of complexes **IV**, **IX**, and **X** at pH 7.0 (Fig. 9): the intensity of the absorption maximum at 470–490 nm decreases within 72 h by 20 (**IV**), 14 (**IX**), and 54% (**X**), respectively.

Complexes **IV**, **IX**, and **X** turned out to be less stable in a phosphate buffer with pH 7.4. After 48 h, these compounds showed a general tendency to decreasing maximum intensity at 470–500 nm by 66–68%.

The earlier studies of the electrochemical properties of the tin(IV) complexes with the Schiff bases [30] showed that these complexes can be involved in the electron transfer reactions at accessible redox potentials to form relatively stable oxidized or reduced forms. A similar behavior assumes that the complexes can react with radical species being involved in chemical or redox reactions. The antiradical activity of complexes **I**–**XIII** in the reactions with $ABTS^{\bullet+}$ and superoxide radical anion generated by the NBT test was studied (Table 5). The known compound Trolox, water-soluble analogue of vitamin E, served as the standard.

Complexes **I**, **III**, **VIII**, and **XIII** bearing *tert*-butyl groups in the Schiff base (L^1, L^4) and alkyl substituents at the tin atom exhibit the highest neutralizing activity in the reaction with the ABTS radical cation. The antiradical capacity of these compounds ($ABTS_{TEAC}$) is comparable with that of Trolox and exceeds it in the case of complex **XIII**. The most part of the diphenyltin derivatives is characterized by high IC_{50} exceeding

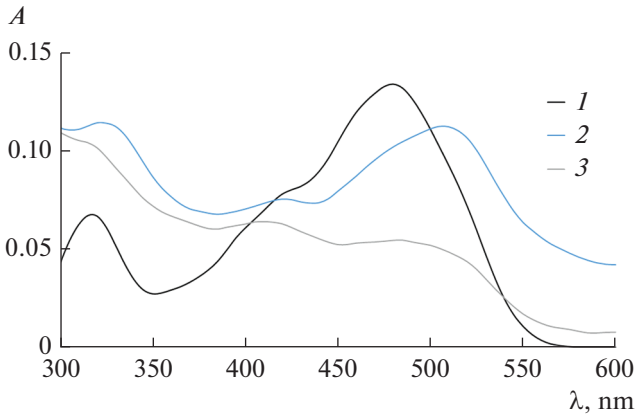

Fig. 7. Electronic absorption spectra of tin(IV) complexes (*1*) **IV**, (*2*) **IX**, and (*3*) **X** (25°C, 3 h, $c = 5 \times 10^{-6}$ mol/L) at pH 4.

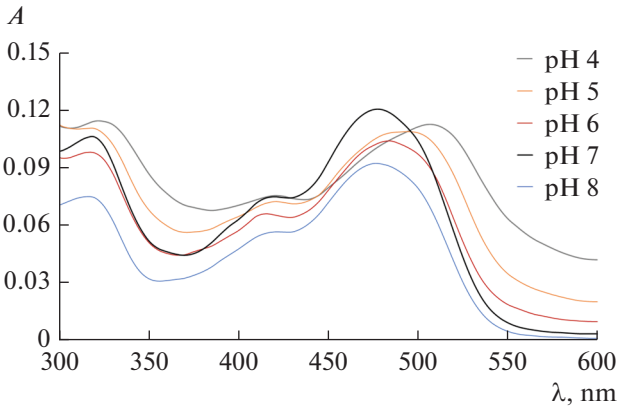

Fig. 8. Electronic absorption spectra of complex **IX** at various pH of the medium (25°C, 3 h, $c = 5 \times 10^{-6}$ mol/L).

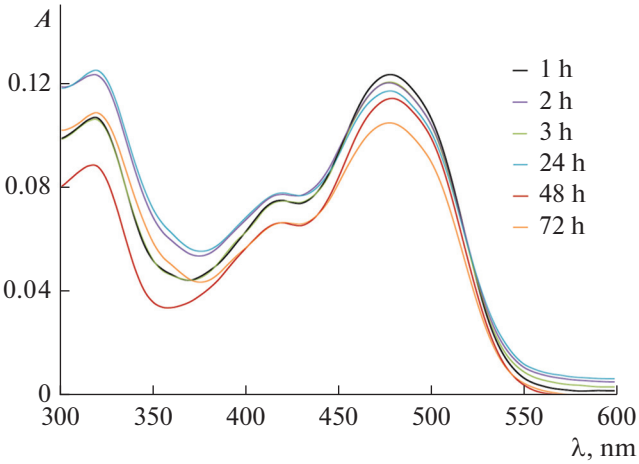

Fig. 9. Change in the electronic absorption spectra of complex **IX** in time at pH 7.0 (25°C, 3 h, $c = 5 \times 10^{-6}$ mol/L).

Table 5. Parameters IC_{50} and $ABTS_{TEAC}$ for complexes **I**–**XIII** in the reactions with the $ABTS^{\bullet+}$ radical cation and superoxide radical anion generated by the xanthine–xanthine oxidase system

Compound	IC_{50} ($ABTS^{\bullet+}$), μM	$ABTS_{TEAC}$	IC_{50} ($O_2^{\bullet-}$), μM
$L^1Sn^nBu_2$ **(I)**	14.5 ± 1.2	0.99 ± 0.11	7.75 ± 0.15
$L^2Sn^nBu_2$ **(II)**	44.5 ± 1.3	0.46 ± 0.03	–
$L^1Sn^tBu_2$ **(III)**	16.4 ± 1.1	1.00 ± 0.05	31.43 ± 0.57
$L^2Sn^tBu_2$ **(IV)**	47.2 ± 0.3	0.45 ± 0.01	>100
$L^3Sn^tBu_2$ **(V)**	56.5 ± 0.1	0.32 ± 0.01	44.40 ± 1.62
L^3SnPh_2 **(VI)**	59.3 ± 1.7	0.36 ± 0.01	27.69 ± 0.71
L^1SnPh_2 **(VII)**	>100	0.05 ± 0.01	35.52 ± 1.12
L^1SnEt_2 **(VIII)**	13.8 ± 0.9	0.92 ± 0.10	26.14 ± 0.54
L^2SnPh_2 **(IX)**	>100	0.20 ± 0.03	29.66 ± 0.37
L^2SnEt_2 **(X)**	96.4 ± 3.6	0.24 ± 0.07	19.16 ± 0.21
L^3SnEt_2 **(XI)**	49.6 ± 2.0	0.40 ± 0.02	>100
L^4SnPh_2 **(XII)**	>100	0.11 ± 0.01	>100
L^4SnEt_2 **(XIII)**	8.4 ± 0.7	1.12 ± 0.08	15.78 ± 0.10
Ph_2SnL^{ONS}*	28.8 ± 0.9	0.62 ± 0.09	7.80 ± 0.23
Ph_2SnL^{ONSCF3}*	25.0 ± 1.3	0.79 ± 0.11	5.16 ± 0.08
Et_2SnL^{ONSCF3}*	35.4 ± 1.8	0.57 ± 0.04	24.02 ± 0.10
Trolox	16.0 ± 1.0	1.00 ± 0.03	62.7 ± 0.60

* The data are taken from [54].

100 μmol/L, which indicates their weak antiradical properties. Note that only IC_{50} reaches 59.3 μmol/L for complex **VI**. A specific feature of complexes **V**, **VI**, and **XIII** with the dichlorosubstituted Schiff base is the absence of a dependence of the radical scavenging activity on the structure of the hydrocarbon groups at the tin atom. Contrarily to compounds **I**, **III**, **VII**, and **X**, complex **XII** is characterized by high IC_{50}, as well as diphenyl derivative **XI**. The replacement of the ethyl groups by butyl groups in complexes **II** and **IV** results nearly in a twofold decrease in IC_{50} and, correspondingly, in an increase in the antiradical activity. The substitution of the donor *tert*-butyl substituents by the chlorine atom or electron-withdrawing nitro group in Schiff base (L^2) for the ethyl-containing tin complexes decreases IC_{50} by an order of magnitude. A similar effect is made by the presence of two chlorine atoms in L^3 favoring a significant decrease in the antiradical activity. A comparative analysis of the previous results for the tridentate O,N,S-donor Schiff bases [56] showed that for complexes **VI**, **VII**, **XI**, and **XII** a change in the O,N,O' coordination mode by O,N,S favored the enhancement of their neutralizing ability toward $ABTS^{\bullet+}$. At the same time, the most active diethyltin derivatives with the O,N,O'-tridentate ligands are characterized by lower values of IC_{50} than that of complex Et_2SnL^{ONSCF3}.

The application of the NBT test makes it possible to estimate the antiradical activity toward the superoxide radical anion generated by the xanthine/xanthine

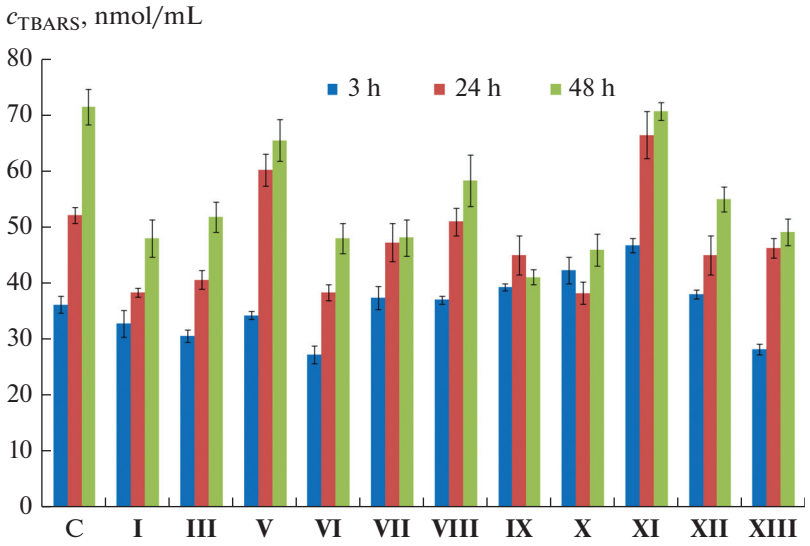

Fig. 10. Change in the TBARS concentration in the Wistar rat liver homogenates in vitro in the presence of complexes **I**, **III**, and **V**–**XIII** during incubation (3, 24, and 48 h) (concentration of the compounds is 100 μmol, C means control (without additives), and average values with standard deviations are presented).

oxidase system. The formation of colored formazan (560 nm) during the enzymatic reaction indicates that the reaction medium contains the superoxide radical anion. The substances inhibiting formazan formation are considered as interceptors of $O_2^{-\bullet}$. The data obtained show that the majority of the tin complexes has neutralizing activity (Table 5) that exceeds the values observed for Trolox. For the compounds with phenyl substituents, IC_{50} varies from 27.69 to 35.52 μmol/L and depends slightly on the nature of substituents in the Schiff base. The replacement of phenyl groups by ethyl groups at the tin atom for the complexes with ligands L^1 and L^2 results in a decrease in IC_{50}, which indicates their higher inhibitory activity. At the same time, an inverse effect is observed on going from the *n*-butyl- to *tert*-butyl-substituted tin derivatives: the antiradical activity decreases. Note that rather low IC_{50} were obtained for the complexes with ethyl groups at the tin atom (**VIII**, **X**, and **XIII**). A series of the compounds (**II**, **IV**, **XI**, and **XII**) is characteristic of the absence of inhibition effect or of a weak neutralizing activity toward $O_2^{-\bullet}$. The minimum IC_{50} was detected for complex **I**. The presence of electron-donating alkyl groups at the tin atom favors a more pronounced antiradical activity toward the superoxide radical anion. For a series of the complexes (**I**, **VIII**, **X**, and **XIII**), the results on the neutralizing activity are comparable with the previously studied tin complexes with the O,N,S-donor Schiff bases [56].

The organotin compounds were shown to exert a pronounced promotion effect on the LP in vitro and act as inductors of the oxidative stress development [57]. To align the negative effect of the organic derivatives of tin, their additives in combination with various antioxidants is frequently applied [58]. The presence of antioxidant groups in the chelating ligands makes it possible to modulate biological activity, including the antiprooxidant properties of the coordination tin compounds. We have recently shown that the tin(IV) complexes with the tridentate O,N,S-donor Schiff bases are characterized by the antioxidant effect in the LP [56]. It seemed interesting to evaluate the influence of the replacement of the O,N,S by O,N,O' coordination mode and the variation of hydrocarbon groups at the tin atom on the antiprooxidant activity of complexes **I**, **III**, and **V**–**XIII** during the prolonged (3, 24, and 48 h) lipid peroxidation in the Wistar rat liver homogenates in vitro. The TBARS concentration, which is a marker of the LP intensity, was determined from a change in the absorbance of the solutions at 535 nm (Fig. 10). The TBARS parameter decreased in the presence of the majority of the studied compounds, which indicates their antioxidant effect. Additives of compounds **V** and **XI** containing chlorine atoms in the Schiff base increased the concentration of the LP products in 24 h, whereas for complex **XI** this effect was also observed at the initial stage (3 h). For compound **V**, an increase in the incubation time (48 h) favors the inversion of its properties to weak antioxidant properties. At the same time, the TBARS concentrations for compound **XI** are comparable with the results of the control experiment.

Compounds **I**, **III**, **VI**, and **XIII** are characterized by a pronounced inhibition effect during the whole time of experiment. A specific feature of complexes **I**, **III**, and **XIII** is the presence of bulky *tert*-butyl groups in the ligands favoring the stabilization of the oxidized forms of the complexes. In the presence of complexes

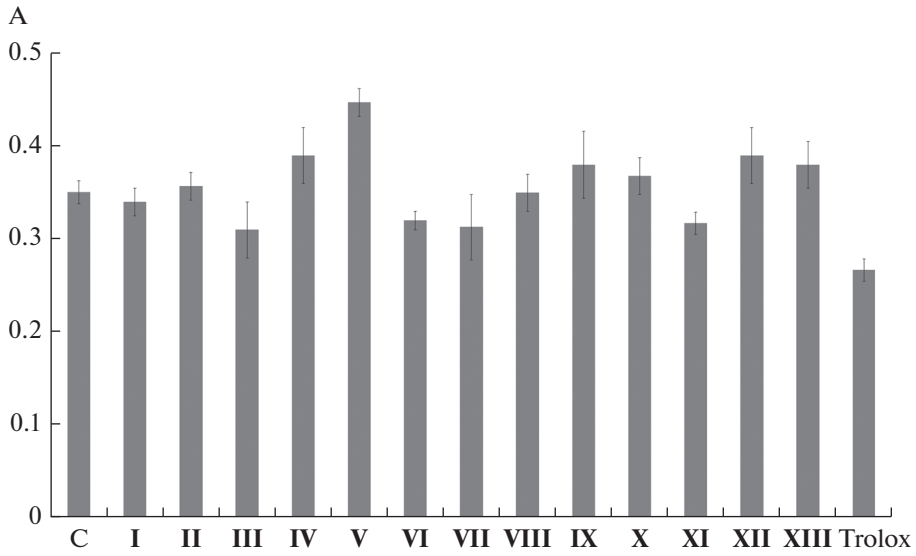

Fig. 11. Change in the absorbance of TBARS formed due to the oxidative DNA damage (2.0 mg mL^{-1}) upon the introduction of the AAPH promotor (40 mmol L^{-1}) in the presence of complexes **I**–**XIII** (50 μmol) and Trolox (C means control, i.e., without additives of compounds).

VIII, **IX**, and **XII**, the initial (3 h) content of TBARS is comparable with that in the control test within the measurement inaccuracy, whereas a weak promotion effect is observed for compound **X**. The antioxidant effect is observed for this group of compounds with an increase in the incubation time. For complexes **IX** and **X**, the TBARS parameter varies in a narrow range of values and is nearly independent of time. A similar behavior indicates the appearance of an induction period during the LP where the TBARS concentration remains at a constant level. The highest antioxidant activity is manifested by the compounds with *tert*-butyl groups in the ligand (**I** and **XIII**) and by compound **VI** combining chlorine atoms in the Schiff base and phenyl substituents at the tin atom. The replacement of the phenyl groups by *tert*-butyl (**V**) or ethyl groups (**XI**) in the complexes containing ligand L^3 results in the intensification of the LP.

Since some compounds exhibit a prooxidant effect on the LP, we studied their influence on the oxidative DNA damage initiated by ROO radicals in vitro. In the presence of AAPH at 37°C, the deoxyribose fragments of DNA molecules are damaged, which favors the violation of the wholeness of the DNA chain. The carbonyl compounds formed during the reaction produce colored TBARS products (λ_{max} = 535 nm) with thiobarbituric acid. The comparative data on the activity of the tin(IV) complexes are presented in Fig. 11.

The results obtained for complex **V** in the reaction with DNA are well consistent with the data on the influence on the LP: a pronounced prooxidant effect is observed in both cases. In the presence of complex **V**, the absorption parameter increases by 27% compared to the control experiment. On the contrary, an insignificant decrease in the TBARS content by 8 and 9% is observed for compounds **VI** and **XI** (with similar Schiff bases), respectively. The promotion of the oxidative DNA damage (11%) is observed for compound **IV** containing *tert*-butyl substituents at the tin atom, as well as for compound **V**. The nature of substituents in the ligands and their number affect the formation of TBARS. In the most cases, the compounds with Schiff base L^1 turned out to be weak LP inhibitors decreasing the TBARS content by 2–10%. At the same time, an insignificant prooxidant effect is observed for the complexes with L^2. In complexes **XII** and **XIII**, an increase in the number of *tert*-butyl groups in the Schiff base also leads to the promotion effect.

It has previously been found that the tin complexes with di- and tridentate Schiff bases exhibit a pronounced antibacterial activity against the gram-positive and gram-negative bacterial strains [56–61]. A similar effect was also expected for the target complexes. The antibacterial activity of the tin(IV) complexes was studied against the bacterial strains *Staphylococcus aureus* ANCC 6538 and *E. faecium* ATCC 3576. Compounds **I**–**III** and **XII** exerted no inhibition effect on the microorganism growth. A very weak bacteriostatic effect on the *S. aureus* strain (MIC = 156.3 ± 1.9 μg/mL) was observed in the cases of complexes **IV** and **VII**–**X**. Similar values of MIC were detected in the case of the *E. faecium* strain for complexes **V**, **VII**, **VIII**, **X**, and **XI**. Complexes **VI** and **XI** with Schiff base L^3 manifested a more pronounced

Table 6. Cytotoxicity IC_{50} (μmol/L) of the studied complexes on various cancer cell lines

Compound	IC_{50}, μmol/L	
	A-549	HCT-116
L^3SnPh_2 (**VI**)	86.6 ± 3.3	39.9 ± 0.9
L^2SnPh_2 (**IX**)	78.1 ± 1.3	54.8 ± 0.1
L^2SnEt_2 (**X**)	64.3 ± 4.1	12.3 ± 0.9
L^3SnEt_2 (**XI**)	40.8 ± 3.2	20.5 ± 0.7
L^4SnPh_2 (**XII**)	141.6 ± 2.1	65.9 ± 1.2
Ph_2SnL^{ONS}*	167.9 ± 9.3	54.6 ± 8.9
Cisplatin*	9.0 ± 0.9	11.2 ± 1.9

* The data are taken from [54].

inhibition activity against the *S. aureus* strain (MIV = 78.1 ± 1.1 μg/mL). In addition to complex **IV**, complex **VI** turned out to be also active toward *E. faecium* (MIC = 78.1 ± 1.7 μg/mL). However, the obtained values of MIC are significantly inferior to that of ciprofloxacin (0.125 μg/mL). The presence of donor *tert*-butyl groups in the Schiff bases together with the chlorine atoms or nitro group results in a considerable decrease in the antibacterial activity of the tin complexes compared to the previously studied compounds containing unsubstituted ligands [59, 61].

The recent attention to the organometallic derivatives of tin(IV) and their coordination compounds is associated with the possibility of their application as potential antiproliferative and anticancer agents, which are an alternative to the platinum drugs [62–64]. Therefore, we studied the antiproliferative activity in vitro of some complexes **VI** and **IX**–**XII** against the A-549 (human alveolar basal epithelium adenocarcinoma) and HCT-116 (human colorectal cancer) cancer cell lines using the MTT test (Table 6). The obtained results indicate a significant enhancement of IC_{50} compared to those of the previously studied related tin(IV) complexes bearing unsubstituted O,N,O'-tridentate Schiff bases [65, 66].

The general tendency to decreasing cytotoxicity of the studied tin complexes is related to the electron-donating *tert*-butyl groups in the ligands. Complex **XII** is distinguished in the series of the studied compounds due to the overestimated values of IC_{50} over those of other compounds. At the same time, the minimum IC_{50} against the considered cell lines are observed for complexes **X** and **XI** with chlorine atoms and nitro groups in the Schiff bases. For the HCT-116 cell line, the cytotoxicity parameters of complex **X** are comparable with the data for cisplatin. The replacement of ethyl groups at the tin atom by phenyl groups in the cases of compounds **VI** and **IX** leads to an increase in the IC_{50}. As a whole, complexes **VI** and **IX** with the O,N,O'-tridentate ligands turned out to be more toxic than the earlier studied diphenyltin(IV) derivatives with the O,N,S-ligands.

Thus, the new tin(IV) complexes with the O,N,O'-donor Schiff bases were synthesized. According to the XRD data, the structure of compound **I** in the crystalline state is dimeric. The coordination sphere of the tin atom is supplemented to the coordination number 6 due to the donor–acceptor interaction with the oxygen atom of the redox-active ligand. Complex $L^2Sn^tBu_2$ is the mononuclear derivative of pentacoordinated tin(IV) with the O,N,O'-tridentate redox-active ligand existing in the dianionic form. The comparative study of the photophysical properties of the synthesized compounds with previously synthesized complexes **VII**–**XIII** showed that all complexes fluoresced at λ_{ex} = 340 nm in the range from 580 to 638 nm. Both the hydrocarbon groups at the tin atom and nature of substituents in Schiff bases affect the position of the emission maximum and relative quantum yield. The maximum relative quantum yields are observed for the complexes with Schiff base L^3 containing chlorine atoms and electron-donating *tert*-butyl groups in the aromatic rings. The energy gap parameters calculated from the spectral data for complexes **I**–**XIII** range from 2.51 to 2.62 eV. The quantum chemical calculations for compounds **VIII**–**XIII** are consistent with the spectral data. An analysis of populations of the Kohn–Sham molecular orbitals for compounds **VIII**–**XIII** showed that the $S_0 \rightarrow S_1$ transitions correspond to the charge transfer between the ligand HOMO and LUMO. The localization of both frontier orbitals in the vicinity of the metal atom is insignificant.

Compounds **I**, **III**, **VIII**, and **XIII** containing *tert*-butyl groups in the Schiff base and alkyl substituents at the tin atom have a more pronounced antiradical activity in the reaction with $ABTS^{\bullet+}$. In the NBT test, the majority of the tin complexes is characterized by the neutralizing activity toward the superoxide radical anion, which exceeds the data for Trolox. The tin(IV) compounds exhibit a dual antiprooxidant activity during the LP of the rat liver homogenates (Wistar) and promoted oxidative DNA damage. The nature of substituents in the ligands and hydrocarbon groups at the tin atom exert a substantial effect on the behavior of the complexes in the LP during the DNA damage.

A weak bacteriostatic effect toward the *Staphylococcus aureus* ANCC 6538 and *E. faecium* ATCC 3576

strains was observed for complexes **IV**–**XI**, whereas compounds **I**–**III** and **XIII** turned out to be inactive. The study of the antiproliferative activity of complexes **VI** and **IX**–**XII** on the A-549 and HCT-116 cell lines made it possible to determine the IC_{50}, which varied from 12.26 to 141.60 μmol/L. The coordination of tridentate Schiff bases L^2H–L^4H bearing different in nature substituents to the organometallic fragment favors a decrease in its toxicity and makes it possible to consider these ligands as efficient modulators of biological properties of coordination compounds. The possibility of exhibiting luminescence activity for similar complexes at moderate cytotoxicity parameters provides prospects for their use in bioimaging.

ACKNOWLEDGMENTS

Quantum chemical calculations and XRD studies were carried out on the equipment of the Center for Collective Use of Physical Methods of Investigation at the Kurnakov Institute of General and Inorganic Chemistry (Russian Academy of Sciences) in the framework of the state assignment of the Kurnakov Institute of General and Inorganic Chemistry (Russian Academy of Sciences) in the field of basic research.

FUNDING

This work was supported by the Russian Science Foundation, project no. 22-13-00118.

CONFLICT OF INTEREST

The authors of this work declare that they have no conflicts of interest.

REFERENCES

1. Baryshnikova, S.V., Poddel'sky, A.I., Bellan, E.V., et al., *Inorg. Chem.*, 2020, vol. 59, no. 10, p. 6774. https://doi.org/10.1021/acs.inorgchem.9b03757
2. Piskunov, A.V., Trofimova, O.Yu., Piskunova, M.S., et al., *Russ. J. Coord. Chem.*, 2018, vol. 44, p. 138. https://doi.org/10.1134/S1070328418020082
3. Baryshnikova, S.V., Bellan, E.V., Poddel'skii, A.I., et al., *Dokl. Chem.*, 2017, vol. 474, p. 101. https://doi.org/10.1134/S0012500817050019
4. Baryshnikova, S.V., Bellan, E.V., Poddel'sky, A.I., et al., *Eur. J. Inorg. Chem.*, 2016, p. 5230. https://doi.org/10.1002/ejic.201600885
5. Ilyakina, E.V., Poddel'sky, A.I., Fukin, G.K., et al., *Inorg. Chem.*, 2013, vol. 52, p. 5284. https://doi.org/10.1021/ic400713p
6. Piskunov, A.V., Trofimova, O.Yu., Fukin, G.K., et al., *Dalton Trans.*, 2012, vol. 41, p. 10970. https://doi.org/10.1039/C2DT30656E
7. Chegerev, M.G. and Piskunov, A.V., *Russ. J. Coord. Chem.*, 2018, vol. 44, no. 4, p. 258. https://doi.org/10.1134/S1070328418040036
8. Piskunov, A.V., Piskunova, M.S., and Chegerev, M.G., *Russ. Chem. Bull.*, 2014, vol. 63, no. 4, p. 912. https://doi.org/10.1007/s11172-014-0527-5
9. Piskunov, A.V., Chegerev, M.G., and Fukin, G.K., *J. Organomet. Chem.*, 2016, vol. 803, p. 51. https://doi.org/10.1016/j.jorganchem.2015.12.012
10. Chegerev, M.G., Piskunov, A.V., Starikova, A.A., et al., *Eur. J. Inorg. Chem.*, 2018, p. 1087. https://doi.org/10.1002/ejic.201701361
11. Klimashevskaya, A.V., Arsenyeva, K.V., Maleeva, A.V., et al., *Eur. J. Inorg. Chem.*, 2023, vol. 26, p. e202300540. https://doi.org/10.1002/ejic.202300540
12. Banti, C.N., Hadjikakoua, S.K., Sismanoglu, T., et al., *J. Inorg. Biochem.*, 2019, vol. 194, p. 114. https://doi.org/10.1016/j.jinorgbio.2019.02.003
13. Zou, T., Lum, C.T., Lok, C.-N., et al., *Chem. Soc. Rev.*, 2015, vol. 44, p. 8786. https://doi.org/10.1039/C5CS00132C
14. Devi, J., Pachwania, S., Kumar, D., et al., *Res. Chem. Intermed.*, 2021, vol. 48, p. 267. https://doi.org/10.1007/s11164-021-04557-w
15. Yusof, E.N.M., Ravoof, T.B.S.A., and Page, A.J., *Polyhedron*, 2021, vol. 198, p. 115069. https://doi.org/10.1016/j.poly.2021.115069
16. Krylova, I.V., Labutskaya, L.D., Markova, M.O., et al., *New J. Chem.*, 2023, vol. 47, p. 11890. https://doi.org/10.1039/d3nj01993d
17. Sanchez-Vergara, M.E., Hamui, L., Gomez, E., et al., *Polymers*, 2021, vol. 13, p. 1023. https://doi.org/10.3390/polym13071023
18. Sánchez-Vergara, M.E., Gómez, E., Dircio, E.T., et al., *Int. J. Mol. Sci.*, 2023, vol. 24, p. 5255. https://doi.org/10.3390/ijms24065255
19. Cantón-Diaz, A.M., Muñoz-Flores, B.M., Moggio, I., et al., *New J. Chem.*, 2018, vol. 42, p. 14586. https://doi.org/10.1039/C8NJ02998A
20. Akbulatov, A.F., Akyeva, A.Y., Shangin, P.G., et al., *Membranes*, 2023, vol. 13, p. 439. https://doi.org/10.3390/membranes13040439
21. Jimenéz-Pérez, V.M., García-Lopez, M.C., Muñoz-Flores, B.M., et al., *J. Mater. Chem. B*, 2021, vol. 3, p. 5731. https://doi.org/10.1039/C5TB00717H
22. López-Espejel, M., Gómez-Treviño, A., Muñoz-Flores, B.M., et al., *J. Mater. Chem. B*, 2021, vol. 9, p. 7698. https://doi.org/10.1039/d1tb01405f
23. Sahu, G., Patra, S.A., Pattanayak, P.D., et al., *Chem. Commun.*, 2023, vol. 59, p. 10188. https://doi.org/10.1039/D3CC01953E
24. Khan, H.Y., Maurya, S.K., Siddique, H.R., et al., *ACS Omega*, 2020, vol. 5, p. 15218. https://doi.org/10.1021/acsomega.0c01206

25. Khatkar, P. and Asija, S., *Phosphorus Sulfur Silicon Relat. Elem.*, 2017, vol. 192, p. 446. https://doi.org/10.1080/10426507.2016.1248762

26. Jiang, W., Qin, Q., Xiao, X., et al., *J. Inorg. Biochem.*, 2022, vol. 232, p. 111808. https://doi.org/10.1016/j.jinorgbio.2022.111808

27. Antonenko, T.A., Shpakovsky, D.B., Vorobyov, M.A., et al., *Appl. Organomet. Chem.*, 2018, vol. 32. p. e4381. https://doi.org/10.1002/aoc.4381

28. Nikitin, E., Mironova, E., Shpakovsky, D., et al., *Molecules*, 2022, vol. 27, p. 8359. https://doi.org/10.3390/molecules27238359

29. Antonenko, A., Gracheva, Y.A., Shpakovsky, D., et al., *Int. J. Mol. Sci.*, 2023, vol. 24, p. 2024. https://doi.org/10.3390/ijms24032024

30. Smolyaninov, I.V., Burmistrova, D.A., Pomortseva, N.P., et al., *Russ. J. Coord. Chem.*, 2023, vol. 49, p. 124. https://doi.org/10.1134/S1070328423700446

31. Smolyaninov, I.V., Poddel'sky, A.I., Burmistrova, D.A., et al., *Molecules*, 2022, vol. 27, p. 8216. https://doi.org/10.3390/molecules27238216

32. Gordon, A.J. and Ford, R.A., *The Chemist's Companion*, New York: Wiley, 1972.

33. Lakowicz, J.R., *Principles of Fluorescence Spectroscopy,* New York: Springer, 2006, 3rd ed.

34. Re, R., Pellergrini, N., Proteggente, A., et al., *Free Radic. Biol. Med.*, 1999, vol. 26, p. 1231. https://doi.org/10.1016/S0891-5849(98)00315-3

35. Sadeer, N.B., Montesano, D., Albrizio, S., et al., *Antioxidants*, 2020, vol. 9, p. 709. https://doi.org/10.3390/antiox9080709

36. Stroev, E.N. and Makarova, V.G., *Praktikum po biologicheskoi khimii* (Laboratory Works in Biological Chemistry), Moscow: Vysshaya shkola, 1986.

37. Zhao, F. and Liu, Z.-Q., *J. Phys. Org. Chem.*, 2009, vol. 22, p. 791. https://doi.org/10.1002/poc.1517

38. *CLSI, Methods for Dilution Antimicrobial Susceptibility Tests for Bacteria That Grow Aerobically. Approved Standards, 10th ed. CLSI document M07-A10*, Wayne, PA, Clinical and Laboratory Standards Institute, 2015.

39. *CrysAlisPro. Version 1.171.38.41*, Rigaku Oxford Diffraction, 2015.

40. Sheldrick, G.M., *SADABS*, Madison: Bruker AXS Inc., 1997.

41. Sheldrick, G.M., *Acta Crystallogr., Sect. C: Struct. Chem.*, 2015, vol. 71, p. 3. https://doi.org/10.1107/S2053229614024218

42. Frisch, M.J., Trucks, G.W., and Schlegel, H.B., *Gaussian 09. Revision D.01*, Wallingford: Gaussian, Inc., 2016.

43. Perdew, J., Ernzerhof, M., and Burke, K., *J. Chem. Phys.*, 1996, vol. 105, p. 9982. https://doi.org/10.1063/1.472933

44. Carlo, A. and Barone, V., *J. Chem. Phys.*, 1999, vol. 110, p. 6158. https://doi.org/10.1063/1.478522

45. Grimme, S., Ehrlich, S., and Goerigk, L., *J. Comput. Chem.*, 2011, vol. 32, p. 1456. https://doi.org/10.1002/jcc.21759

46. Tomasi, J., Mennucci, B., and Cammi, R., *Chem. Rev.*, 2005, vol. 105, p. 2999. https://doi.org/10.1021/cr9904009

47. Basu, S., Masharing, C., and Das, B., *Heteroat. Chem.*, 2012, vol. 23, p. 457. https://doi.org/10.1002/hc.21037

48. Basu, S., Gupta, G., Das, B., et al., *J. Organomet. Chem.*, 2010, vol. 695, p. 2098. https://doi.org/10.1016/j.jorganchem.2010.05.026

49. Farfan, N., Mancilla, T., Santillan, R., et al., *J. Organomet. Chem.*, 2004, vol. 689, p. 3481. https://doi.org/10.1016/j.jorganchem.2004.07.053

50. Tan, Y.-X., Zhang, Zh.-J., Liu, Y., et al., *J. Mol. Struct.*, 2017, vol. 1149, p. 874. https://doi.org/10.1016/j.molstruc.2017.08.058

51. Garcia-Lopez, M.C., Munoz-Flores, B.M., Jimenez-Perez, V.M., et al., *Dyes Pigm.*, 2014, vol. 106, p. 188. https://doi.org/10.1016/j.dyepig.2014.02.021

52. Beltran, H.I., Damian-Zea, C., Hernandez-Ortega, S., et al., *J. Inorg. Biochem.*, 2007, vol. 101, p. 1070. https://doi.org/10.1016/j.jinorgbio.2007.04.002

53. Gonzalez-Hernandez, A. and Barba, V., *Inorg. Chim. Acta*, 2018, vol. 483, p. 284. https://doi.org/10.1016/j.ica.2018.08.026

54. Vinayak, R., Dey, D., Ghosh, D., et al., *Appl. Organomet. Chem.*, 2018, vol. 32, p. e4122. https://doi.org/10.1002/aoc.4122

55. Budnikova, Y.H., Dudkina, Y.B., Kalinin, A.A., et al., *Electrochim. Acta*, 2021, vol. 368, p. 137578. https://doi.org/10.1016/j.electacta.2020.137578

56. Smolyaninov, I.V., Poddel'sky, A.I., Burmistrova, D.A., et al., *Int. J. Mol. Sci.*, 2023, vol. 24, no. 9, p. 8319. https://doi.org/10.3390/ijms24098319

57. Petrosyan, V.D., Milaeva, E.R., Gracheva, Yu.A., et al., *Applied Organomet. Chem.*, 2002, vol. 16, p. 655. https://doi.org/10.1002/aoc.360

58. Antonova, N.A., Kolyada, M.N., Osipova, V.P., et al., *Dokl. Chem.*, 2008, vol. 419, p. 62. https://doi.org/10.1134/s0012500808030051

59. Devi, J., Yadav, J., and Singh, N., *Res. Chem. Intermed.*, 2019, vol. 45, p. 3943. https://doi.org/10.1007/s11164-019-03830-60

60. Devi, J., Pachwania, S., Kumar, D., et al., *Res. Chem. Intermed.*, 2022, vol. 48, p. 267. https://doi.org/10.1007/s11164-021-04557-w

61. Devi, J., Pachwania, S., Yadav, J., et al., *Phosphorus, Sulfur Silicon Relat. Elem.*, 2021, vol. 196, p. 119. https://doi.org/10.1080/10426507.2020.1818749

62. Devi, J. and Yadav, J., *Anti-Cancer Agents Med. Chem.*, 2018, vol. 18, p. 335. https://doi.org/10.2174/1871520617666171106125114
63. Banti, C.N., Hadjikakou, S.K., Sismanoglu, T., et al., *J. Inorg. Biochem.*, 2019, vol. 194, p. 114. https://doi.org/10.1016/j.jinorgbio.2019.02.003
64. Milaeva, E.R., Shpakovsky, D.B., Gracheva, Y.A., et al., *Pure Appl. Chem.*, 2020, vol. 92, no. 8, p. 1201. https://doi.org/10.1515/pac-2019-1209
65. Beltran, H.I., Damian-Zea, C., Hernández-Ortega, S., et al., *J. Inorg. Biochem.*, 2007, vol. 101, p. 1070. https://doi.org/10.1016/j.jinorgbio.2007.04.002
66. Vinayak, D., Dey, D., Ghosh, D., et al., *Appl. Organomet. Chem.*, 2017, p. e4122. https://doi.org/10.1002/aoc.4122

Translated by E. Yablonskaya